Pergamon

PII: S0301-9322(96)00029-8

Int. J. Multiphase Flow Vol. 22, No. 5, pp. 829–848, 1996
Copyright © 1996 Elsevier Science Ltd
Printed in Great Britain. All rights reserved
0301-9322/96 $15.00 + 0.00

RELATION OF DEPOSITION TO DROP SIZE WHEN THE RATE LAW IS NONLINEAR

K. J. HAY†, ZI-CHAO LIU and T. J. HANRATTY
Department of Chemical Engineering, University of Illinois, Urbana, IL 61801, U.S.A.

(Received 11 May 1995; in revised form 22 February 1996)

Abstract—Measurements of drop size distributions have been obtained by photography for air–water annular flow in a 4.2 cm vertical pipe. Results are presented for a constant superficial gas velocity (36 m/s) for different liquid flows. It is shown that droplet deposition rates can be interpreted by relating the deposition constant directly to the root-mean square of the velocity fluctuations of the drops. The observed decrease of the deposition constant with increasing liquid flow cannot be explained by an increase in drop size. It is suggested that droplet–droplet interactions cause a decrease in drop turbulence. Copyright © 1996 Elsevier Science Ltd.

Key Words: annular flow, drop size, deposition, particle interactions

1. INTRODUCTION

In the annular regime, that occurs when gas and liquid flow through a vertical pipe, part of the liquid moves as a layer along the wall and part as droplets in the gas. A central problem is the prediction of the entrainment, $E = W_{LE}/W_L$, where W_{LE} is the weight flow of entrained drops and W_L is the total weight flow of liquid. A popular approach is to describe E as resulting from a balance between the rate of atomization of the liquid layer, R_A, and the rate of deposition of droplets, R_D.

Usual practice has been to relate the rate of deposition to the mass concentration of droplets, C_B, as

$$R_D = k_D C_B = k_D \frac{W_{LE}}{SQ_G}. \quad [1]$$

Here Q_G is the volumetric gas flow and S is the average ratio of the droplet velocity and the axial velocity of the gas. The rate of deposition can be described in terms of the average velocity with which droplets strike the boundary, V_W, so that

$$R_D = V_W C_W = V_W C_B \frac{C_W}{C_B}, \quad [2]$$

where C_W is the drop concentration at the wall. Measurements presented by Gill *et al.* (1964) and in this paper show that $C_W/C_B \approx 1$ so that $k_D = V_W$ if k_D is defined in terms of C_B, rather than $(C_B - C_W)$.

In annular flows droplets strike the boundary by a free-flight. Binder & Hanratty (1991) have argued that the average velocity of the particles at the point from which they start their free-flight is given by

$$k_D = f\sqrt{\frac{2}{\pi}}(\overline{v_p^2})^{1/2} \quad [3]$$

if the turbulent velocity fluctuations of the particles may be approximated by a Gaussian distribution. Here $(\overline{v_p^2})^{1/2}$ is the root-mean square of the turbulent velocity fluctuations of the drops and $\sqrt{2/\pi}(\overline{v_p^2})^{1/2}$ is the mean magnitude. Term f is the fraction of the particles which are moving toward the wall at the average location from which the particles are launched on a free-flight. One

†Currently at U.S. Army Construction Engineering Research Laboratories, Champaign, IL 61826, U.S.A.

of the important results of this paper is the verification of [3] for dilute concentrations of drops. A more detailed discussion of [3] is given by Lee *et al.* (1989a).

Recent measurements of R_D by Schadel *et al.* (1990) and by Govan *et al.* (1988), as well as earlier measurements by Namie & Ueda (1972) and by Andreussi & Zanelli (1976), show that k_D varies with concentration. Some of these results are shown in figure 1. At low concentrations, R_D varies linearly with C_B. At high concentrations, the rate of deposition is a constant or $k_D \sim (C_B)^{-1}$. From [3], one would conclude that $(\overline{v_p^2})^{1/2}$ varies as $(C_B)^{-1}$ at large C_B, if droplet turbulence continues to control deposition at large C_B.

One possible explanation for this behavior is that droplet coalescence results in the formation of large sluggish droplets which have very small $(\overline{v_p^2})^{1/2}$. Figure 1 would then be explained if there is a critical droplet concentration, beyond which further addition of liquid to the gas phase produces large drops but does not result in larger deposition rates. The study described in this paper was undertaken to test this idea.

The system considered is upward flow of air and water in the 4.2 cm pipe in which Schadel *et al.* (1990) carried out their experiments. Drop size distributions were measured close to the outlet for a superficial gas velocity of 36 m/s and for liquid mass flow rates of 30 g/s to 170 g/s. In one experiment, drop sizes were measured at two locations along the pipe to see how the distribution evolves.

Drop sizes in annular flows have been measured with laser-diffraction methods (Azzopardi *et al.* 1978, 1980, 1991; Azzopardi 1985; Jepson *et al.* 1989), the phase-Doppler technique (Azzopardi & Teixeira 1992), the laser-grating technique (Semiat & Dukler 1981; Lopes & Dukler 1986; Fore & Dukler 1995), electrical contact methods (Wicks & Dukler 1966; Tatterson *et al.* 1977) and droplet immersion methods (Namie & Ueda 1972; Okada *et al.* 1995). Direct *in situ* photography was used in this study. This has the disadvantage that the analysis of photographs is time consuming. However, there were a number of compelling reasons for using this approach: liquid configurations other than spherical drops could be detected, the distribution function is measured

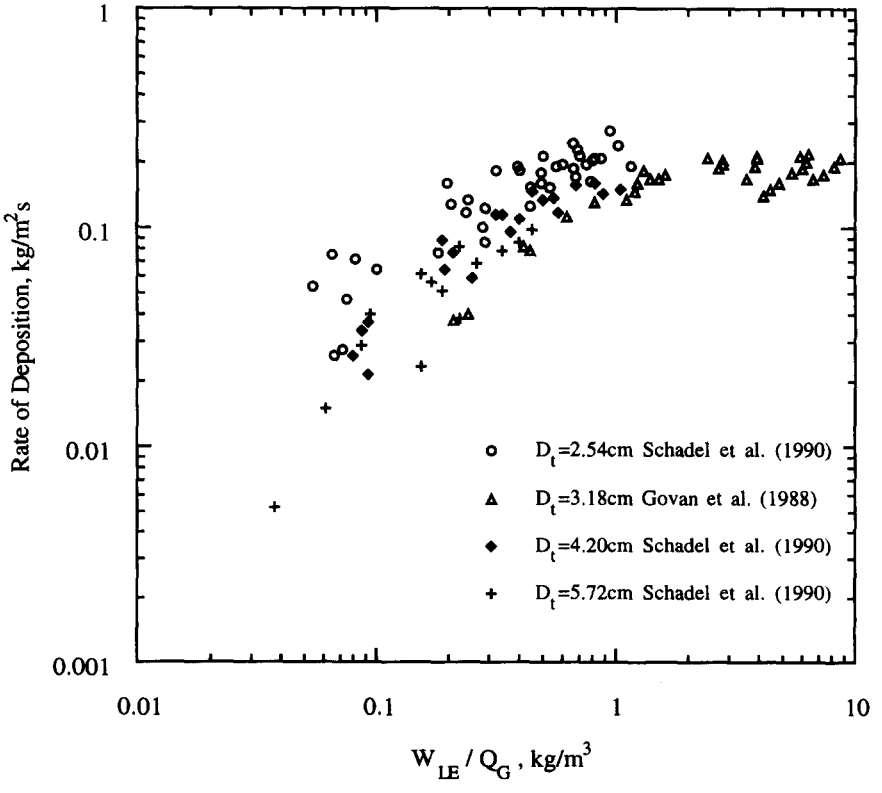

Figure 1. Effect of concentration ($S = 1$) on deposition.

directly (and not assumed *a priori*) and diffraction methods become less accurate as the drop size increases.

The experiments show that the original supposition, outlined above, is incorrect. Drop size increased with increasing liquid flow rate, but not enough to account for the decrease in $(\overline{v_p^2})^{1/2}$ suggested by the measurements of R_D. A new explanation is proposed, but not substantiated, by which droplet–droplet encounters cause $(\overline{v_p^2})^{1/2}$ to decrease as $(C_B)^{-1}$ at large concentrations.

2. THEORY—DILUTE SUSPENSIONS

If the droplet concentration is dilute enough that droplet–droplet interactions are not important, the rate of deposition can be estimated from [3] by taking $f = 1/2$ and by assuming that $\overline{v_p^2}$ can be obtained by considering the statistical behavior of single drops in a turbulent field. For the experiments being considered, the drops have enough inertia that they move through the viscous wall region in free-flight but not enough inertia that the free-flight extends from wall to wall (see Binder & Hanratty 1991). Consequently, the drops are undergoing a haphazard motion caused by the gas phase turbulence. Nonhomogeneities in the gas phase turbulence close to the wall are having little effect so $\overline{v_p^2}$ may be taken as an average over the pipe cross-section. Furthermore, lift effects associated with mean velocity gradients (Lee & Durst 1982) are ignored.

The reciprocal time constant, which characterizes the ability of drops to follow fluid turbulence is defined as

$$\beta = \frac{3C_D\rho_f}{4d_p\rho_p} V_S, \qquad [4]$$

where C_D is the drag coefficient, d_p, the drop diameter and V_S, the mean relative velocity between the drops and the gas. Reeks (1977) and Mei *et al.* (1993) have presented analyses for $\overline{v_p^2}/\overline{v_f^2}$ for a homogeneous isotropic turbulence, where $\overline{v_f^2}$ is the mean square of the fluid turbulent velocity fluctuations. The parameters affecting the particle turbulence are shown to be $V_S/(\overline{v_f^2})^{1/2}$ and $\beta/(\overline{v_f^2})^{1/2}k_0$ where $(\overline{v_f^2})^{1/2}k_0$ is the reciprocal of a characteristic time scale of the fluid turbulence.

Vames & Hanratty (1988) measured $\overline{v_p^2}$ for particles in a fluid flowing turbulently through a pipe, under conditions that $V_S/(\overline{v_f^2})^{1/2}$ was having a small effect. Good agreement between these measurements and Reek's analysis is obtained if $[(\overline{v_f^2})^{1/2}k_0]^{-1}$ is taken as equal to the Lagrangian time scale of the fluid, τ_{LF} (Hay 1994). By making this substitution, [3] and the analyses by Reeks (1977) and Mei *et al.* (1993) can be used to calculate k_D for dilute concentrations. The chief difficulty with this approach is the estimation of $V_S/(\overline{v_f^2})^{1/2}$.

3. DESCRIPTION OF EXPERIMENTS

3.1. Impact tube experiments

The equipment used in the experiments is described in previous papers by Asali *et al.* (1985a) and by Schadel *et al.* (1990). The air and water entered at the bottom of the 4.2 cm pipe. The water was introduced as a wall film by a slotted entrance described by Asali (1984).

Droplet fluxes and impact pressures were measured 5.29 m above the entrance. The test section consisted of a straight Plexiglas pipe with ports at two axial locations. The lower port accommodated a pressure tap. An impact tube constructed of 1/8 inch stainless steel tubing entered through the upper port and faced upstream. The end of the tube was beveled; its inside diameter was measured as 1.457 ± 0.004 mm.

Local droplet fluxes, G_{LE}, were determined by withdrawing liquid through the tube. The flux was calculated as the measured mass flow of the liquid divided by the inside area. Williams (1990) and Asali (1984) tested the accuracy of this method by comparing measured fluxes obtained with tubes of different diameter. The total entrainment, E, was calculated from measured droplet fluxes at

different locations over a traverse from the pipe center to the time-averaged location of the liquid film, m:

$$E = \frac{2\pi a^2}{W_L} \int_0^{1-m/a} G_{LE} \frac{r}{a} d\left(\frac{r}{a}\right), \quad [5]$$

where a is the pipe radius. Measurements could not be made too close to the film so an extrapolation of G_{LE} to $(a - m)$ had to be made. This was the chief source of error (about 6%) in the determination of E.

Measurements of the difference in pressure at the pitot opening and at the pressure tap on the wall, were used to calculate gas velocity profiles by using the following equation derived by Anderson & Mantzouranis (1960):

$$\Delta P = \tfrac{1}{2}\epsilon\rho_G U^2 + \alpha S U G_{LE}, \quad [6]$$

where U is the local time–mean gas velocity, ϵ is the void fraction, and α is the momentum transfer factor. For these experiments, all drops moving towards the pitot tube opening were captured, $\alpha = 1$. Direct measurements of the slip ratio were not made. However, data of Teixeira (1988) indicate that it does not vary appreciably with location. Therefore, the procedure described in detail by Williams (1990) and Williams *et al.* (1996) was used. The slip ratio was assumed to be constant over the entire pipe cross-section and was adjusted until the integrated gas phase velocity profile agreed with the measured gas flow rate. As with the droplet flux profiles, an extrapolation was made to $(a - m)$.

Concentration profiles were calculated by dividing the local droplet flux by the local drop velocity:

$$C = \frac{G_{LE}}{SU}. \quad [7]$$

3.2. Drop size measurements

A Molectron MY 34 Nd:YAG pulsed laser was used to illuminate a plane parallel to the flow direction. Drops were photographed with an Olympus 35 mm camera aimed perpendicular to the flow direction, as shown by figure 2. A special three armed test section was constructed to allow viewing of the entrained drops. The liquid film was removed with an adjustable slotted section with an 1/8 inch protruding sharp lip that was located approximately one pipe diameter below the test volume. Measurements were taken at the center of the flow to avoid the possibility of unwanted effects introduced by the withdrawal.

The laser can deliver a 225 mJ pulse at a wavelength of 532 nm with a duration of 15 ns, during which a droplet moves less than one micron. The horizontal dimension of the 8 mm circular beam was contracted to less than 2 mm at the center of the test section by using special optics described by Hay (1994). The ability to keep the laser sheet thin is an important advantage of this technique because the effective depth of field will be no more than this thickness. By setting the optics of the camera in such a way as to give a depth of field greater than the sheet thickness, concern over the effects of droplet size on depth of field was lessened.

The camera had a long adjustable bellows attached to a 85–200 mm Kyron lens set at 180 mm. It was mounted on a traversing platform which allowed movement towards the test section to adjust the focal plane location as well as to adjust the height and the aim. The aperture f number was set at 22. The arrangement gave a measured magnification of 3.10 and a calculated depth of field of 1.8 mm. Kodak T-Max 35 mm 400 ASA black and white film was used which provided a good compromise between speed and resolution.

During an experiment, the camera shutter was opened and closed briefly while one laser pulse was triggered manually. Photographs were taken at a rate of about one per two seconds, so one roll of 24 exposures were exposed in less than one minute. All photographs were taken in a single experiment to ensure that conditions were constant.

The photographic negatives lacked sufficient contrast to determine drop edges confidently so the contrast was increased by making positives. A Mitutoyo PJ311 profile projector with 1 μm

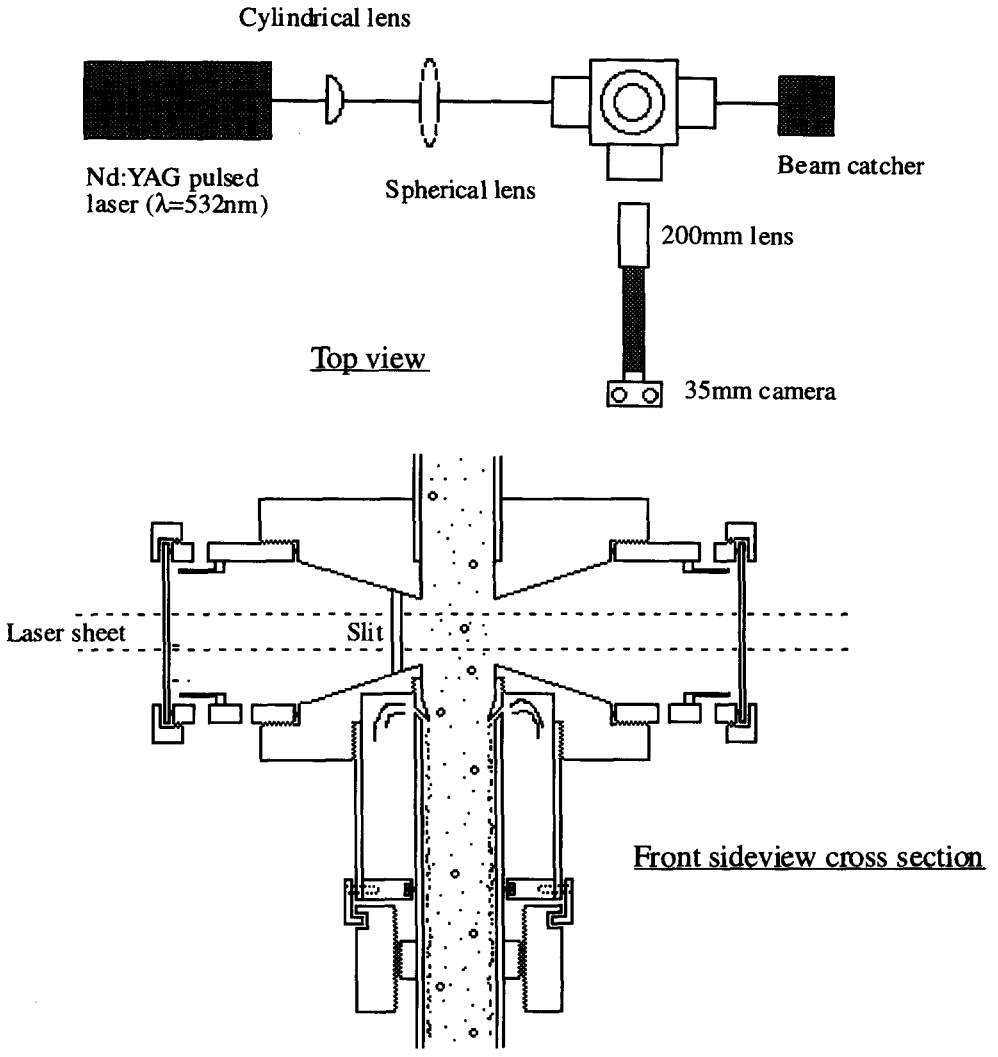

Figure 2. Pulsed laser sideview setup.

precision was used to analyse each photograph. The projector equipment consists of a cross travel stage with micrometer adjusters for two dimensions, a zoom lens capable of 10–50 times magnification, a digital counter readout and a computer interface. The positives were placed on the stage in a fixed position and analysed in a methodical back and forth technique to prevent missing or measuring droplets more than once. The photographs were roughly 24 mm high and 36 mm wide so that, considering the magnification, the actual test volume dimensions were roughly 7.7 mm by 11.6 mm by the effective depth of field. As mentioned before, the depth of field in this case depends on the thickness of the laser sheet in the test volume; this is difficult to measure with precision. However, it can be calculated by adjusting its value until the droplet concentration found with the photographs matches concentrations measured in the pitot experiments.

Most of the exposures on a given photograph were due to scatter off drop surfaces. As a result, a typical drop image resembled two half-moons facing each other. The left half-moon was formed from the incident beam reflecting off the left side. The right half moon was formed by light transmitted through the drop and angled toward the camera by the drop's right edge. This gives clear images of the two horizontal edges of the drops, so that drop diameters were obtained by measuring the horizontal distance between the outermost edges. This is based on the assumption that drops are spherical. Only a few images, mostly for large drops above 350 μm, appeared to be nonspherical.

The only two criteria, for selecting droplets to measure, were that the edges of the drop must be visible and focused. These criteria were not met in situations where a drop was only partially illuminated at the edge of the laser sheet, when an out of plane drop was illuminated by direct blocking of an in plane drop or when a drop was illuminated by scattered light. As expected, all of these effects tend to increase with increasing drop concentration. At higher concentrations, there is also an increased risk that the view of illuminated small droplets (< 30 μm) becomes obstructed. In an effort to avoid these problems, photographs that showed large areas of obstructed view were not analysed.

To obtain accurate mass distributions, either an enormous number of drops need to be measured or a method needs to be developed to improve the statistical representation of large drops. Because the droplet photographs were analysed manually, the latter approach was more feasible. For each flow condition, one set of photographs was scanned for all measurable drops (small drop analysis, SA). A second set of photographs were scanned for larger drops (large drop analysis, LA). The cutoff diameter was 160–200 μm but remained constant for a particular flow condition. In order to obtain drop samples from many photographs, only a one centimeter horizontal strip across the center of each photograph was used in the small drop analysis. In the large drop analysis, drops were compared to a gauge, placed on the projector, which was slightly less than the cutoff width. This ensured that all drops at or above the cutoff were measured. Measured drops were sorted into equal-sized drop size bins of 20 μm. The numbers of drops with diameters below or equal to the cutoff diameter, that were counted in the small drop analysis, were used to calculate the distribution function. The numbers of drops in the distribution with diameters above the cutoff diameter were obtained by using a weighting calculation. This weighting was based on the proportionate amount of photograph volume scanned. For bins with median diameters below the cutoff diameter, this volume was the volume scanned in the small analysis. For bins with median diameters above the

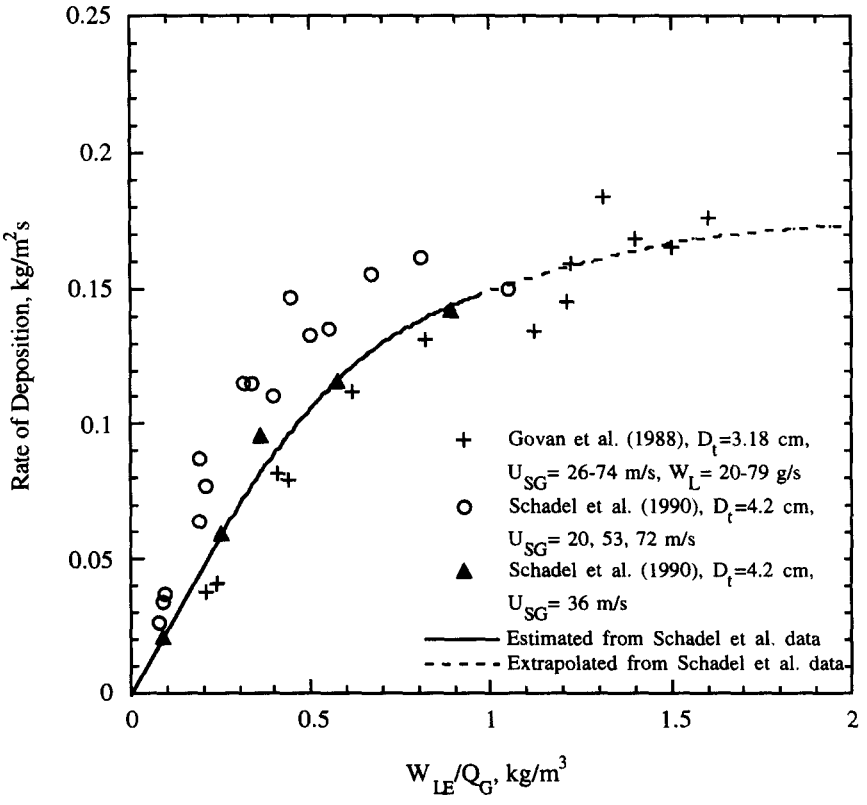

Figure 3. Estimation of rates of deposition.

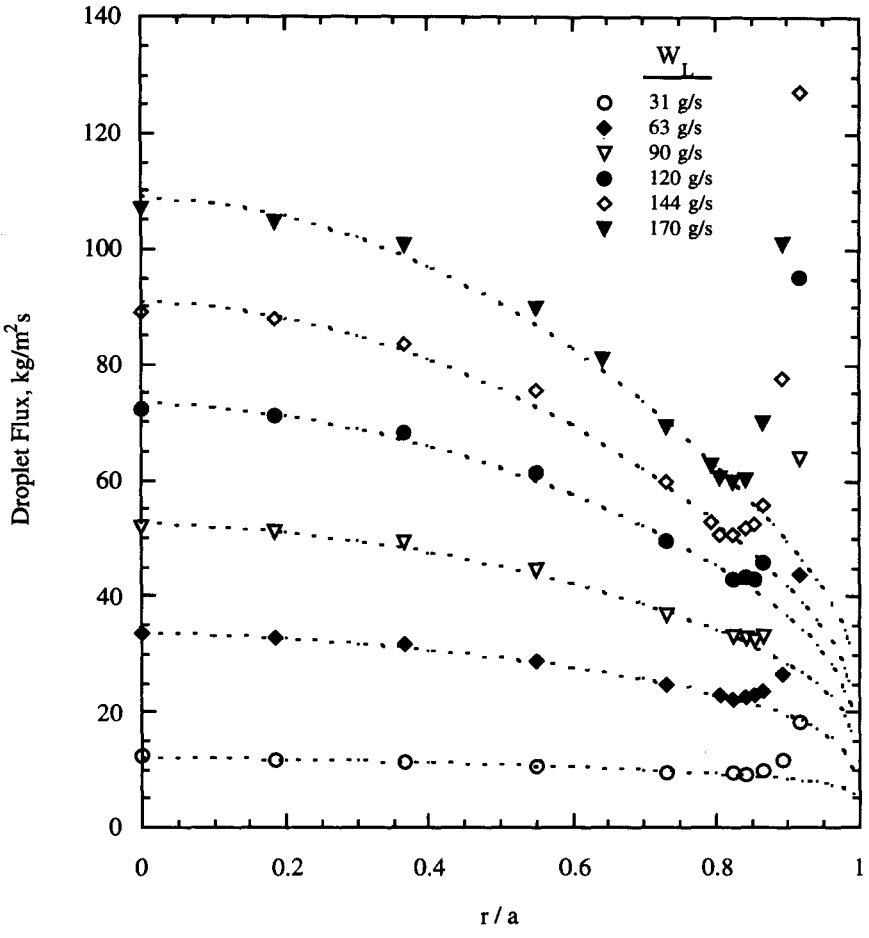

Figure 4. Droplet flux profiles.

cutoff diameter, this volume was the sum of the volumes scanned by both analyses. A population distribution was calculated by the following equations:

$$N(i) = \frac{n_{SA}(i)}{V_{SA}}, \quad \text{for } d(i) \leqslant \text{cutoff}; \tag{8}$$

$$N(i) = \frac{n_{SA}(i) + n_{LA}(i)}{V_{SA} + V_{LA}}, \quad \text{for } d(i) > \text{cutoff}, \tag{9}$$

where $N(i)$ = drop population per volume for the ith bin; $n(i)$ = number of drops in the ith bin; $d(i)$ = median diameter of the ith bin and V = volume scanned for drops in photographs. A typical sample for a given flow condition was between 2400 and 4100 drops.

A reasonable estimate of the error for an individual drop measurement is of the order of $\pm 10\,\mu$m. This is the main reason for distributing the drop measurements into bins of $20\,\mu$m

Table 1. Measured entrainment and relative velocity ratios

W_L (g/s)	E	S
31	0.419	0.82
63	0.527	0.79
90	0.553	0.79
119	0.558	0.77
144	0.564	0.74
170	0.570	—

increments. The error in determining the Sauter mean, is in the order of 6 to 7%; however, this is a conservative estimate because of the use of a separate analysis for the large drops.

4. RESULTS

Results were obtained for conditions represented by the darkened triangles in figure 3. These are rates of deposition measured by Schadel *et al.* (1990) for a tube diameter of 4.2 cm and superficial gas velocity of 36 m/s. The dashed curve is an extrapolation of these data that is consistent with measurements obtained under other conditions by Govan *et al.* (1988) and Schadel *et al.* (1990).

4.1. Impact tube results

Droplet flux measurements are plotted in figure 4. These show a maximum value near the center of the pipe ($r = 0$). The flux also shows a sharp increase near the pipe wall where the pitot tube intercepts waves on the liquid film. The dashed curve is an extrapolation from the point where the tube intercepts waves to the average film thickness. The shapes of the flux profiles are similar for different liquid flows. These profiles were integrated, as indicated by [5] to obtain the results presented in table 1.

The relative velocity ratios, calculated in the determination of the gas velocity profiles, are also presented in table 1. These values of S are smaller than would be determined from the free-fall velocities. Schadel *et al.* (1990) have suggested that the drops are not in the flow long enough to accelerate to the gas velocity and used this concept to calculate values of S for $U_{SG} = 36$ m/s that

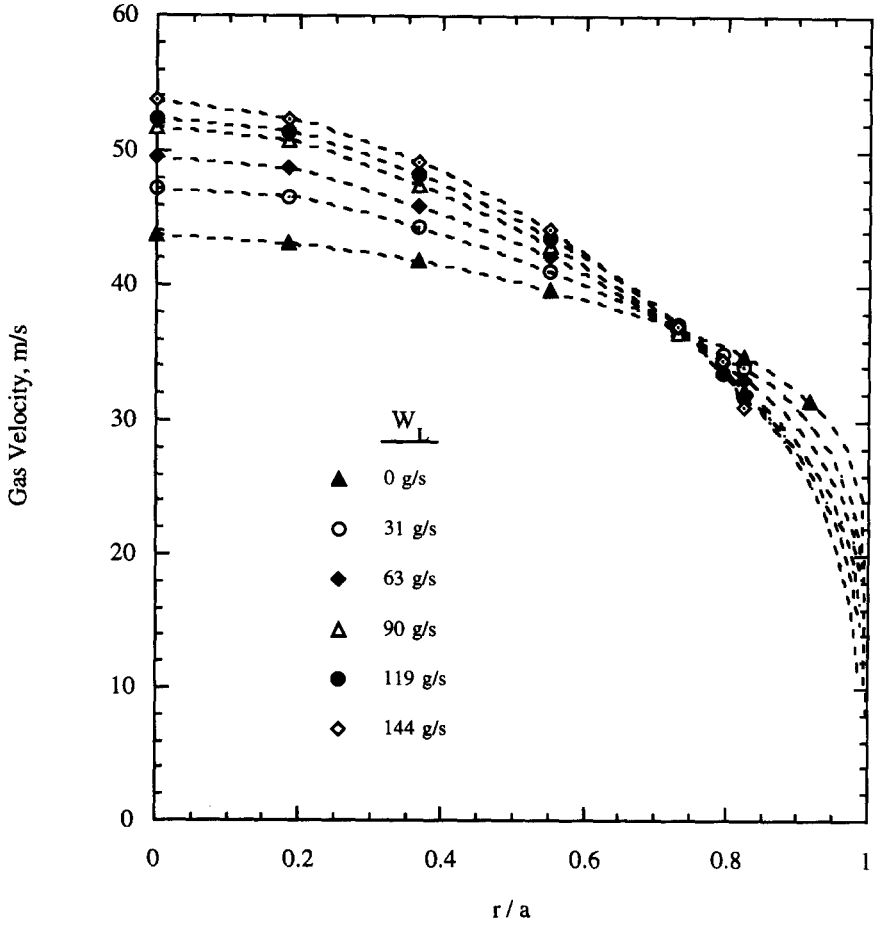

Figure 5. Gas velocity profiles.

varied from 0.75 to 0.70 as the liquid flow increased from 20 to 93 g/s. Teixeira (1988) and Fore & Dukler (1995) measured drop velocities directly, and obtained values of S close to those presented in table 1.

Gas velocity profiles, in figure 5, show a definite change in shape with increases in the liquid flow rate. The flat turbulent profile for single-phase flow develops, with increasing liquid flow, into a more diffuse profile. Two factors could contribute to this change in the velocity profile, changes in the gas–liquid film interface and increases in drop concentration. A plot in accordance with the velocity defect law (Schlichting 1968) gives an indication of the role of the film on the wall in affecting the velocity field. If the film acts on the gas core in a way similar to that of a roughened boundary, then curves of $(u_c - u)/u^*$ versus r/a at different liquid flow rates would fall on the same curve (u_c is the centerline gas velocity and u^* is the friction velocity calculated with the correlation of Asali *et al.* 1985b). Figure 6 shows that this is the case and suggests that there is an increase in gas phase turbulence, due primarily to changes in the roughness of the interface, if the root-mean square gas phase velocity fluctuations increase with u^*.

Drop velocities are calculated as the product of the relative velocity ratios and the gas velocities. The concentration profiles, shown in figure 7, were obtained by dividing droplet fluxes by droplet velocities. These are approximately constant over the pipe cross-section, in agreement with the findings of Gill *et al.* (1964). This indicates that turbulent diffusion to the wall is rapid enough that it is not affecting droplet deposition.

4.2. Drop size results

Table 2 gives the number of photographs and drops analysed for each condition. Increases in drop size are found with increasing liquid flow. Here d_{32}, d_{30} and $d_{50\%}$ are, respectively, the Sauter, volume mean and volume median diameters. Cumulative volume distributions are plotted in figure 8. The increasing contribution to the entrained mass by larger drops is clearly demonstrated.

For the range of flow conditions used in this study, the probability density functions are best characterized by the log normal and upper-limit log normal relations, used by Wicks & Dukler (1966), Tatterson *et al.* (1977) and Andreussi *et al.* (1978) for annular flow. Distribution functions

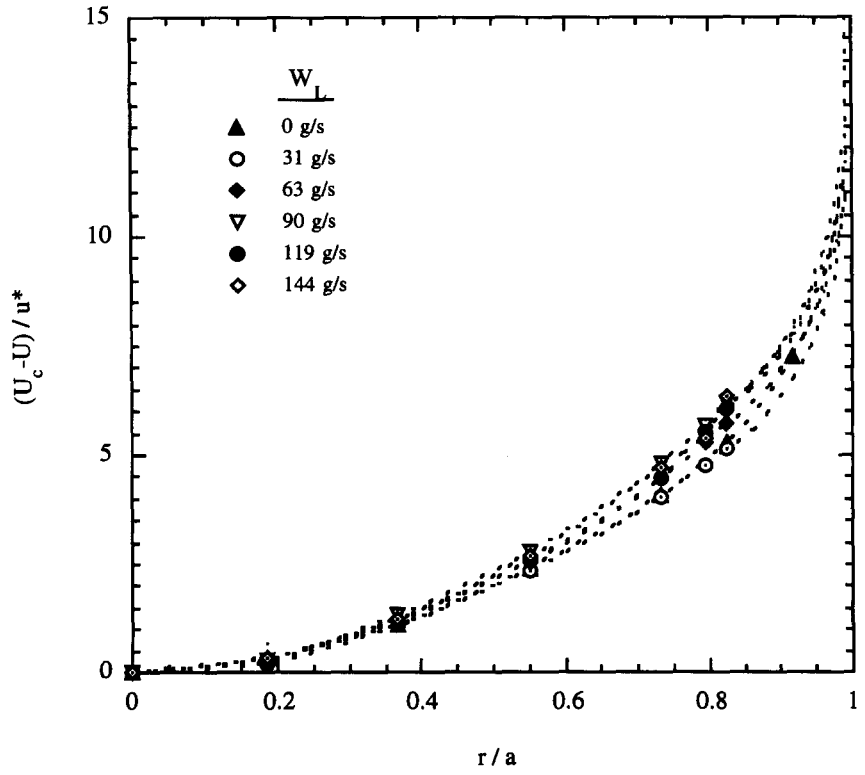

Figure 6. Universal gas velocity profiles.

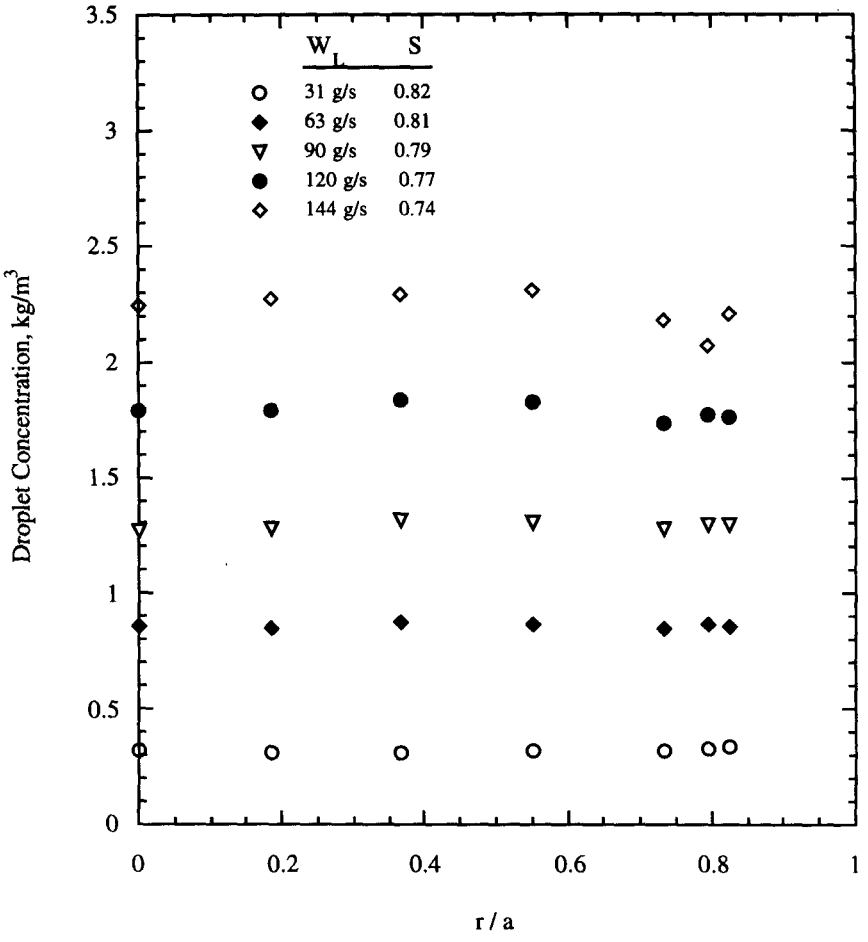

Figure 7. Droplet concentration profiles.

with two peaks, such as obtained by Fore & Dukler (1995), were not observed. The Rosin–Rammler distribution function, used by Azzopardi *et al.* (1978, 1980, 1991), Azzopardi (1985), Teixeira (1988) and Jepson *et al.* (1989), fits the cumulative volume distributions for $W_L \geqslant 90$ g/s but not the probability distribution function, as is illustrated in figure 9 for $W_L = 144$ g/s. The Rosin–Rammler distribution underpredicts the contribution by large drops, especially at lower liquid flow rates. Figure 10 shows the fit to the data in figure 9 with an upper limit log normal distribution. Table 3 presents the distribution parameters for the log normal and the upper limit log normal distributions for all of the flow conditions that were studied.

Azzopardi (1985) has suggested the following equation for predicting the Sauter mean diameter:

$$\frac{d_{32}}{\lambda} = \frac{15.4}{\mathrm{We}^{0.58}} + 3.5\,\frac{G_{LE}}{\rho_L U}, \qquad [10]$$

where G_{LE} is the entrained liquid mass flux and We is a Weber number based on U and $\lambda = (\sigma/\rho_L g)^{1/2}$. A comparison of this equation with the measurements obtained in this study is

Table 2. Photograph samples and mean drop diameters

W_L (g/s)	No. photos Small analysis	No. drops	No. photos Large analysis	Cutoff d (μm)	No. drops >cutoff	d_{32} (μm)	d_{30} (μm)	$d_{50\%}$ (μm)
30	19	2301	64	160	109	82.0	107	81.8
60	16	2967	51	180	222	102	133	110
90	12	2522	21	200	146	118	158	135
120	10	2578	30	160	641	126	172	153
144	12	3183	32	160	873	138	189	165
170	7	2120	10	160	328	146	206	181

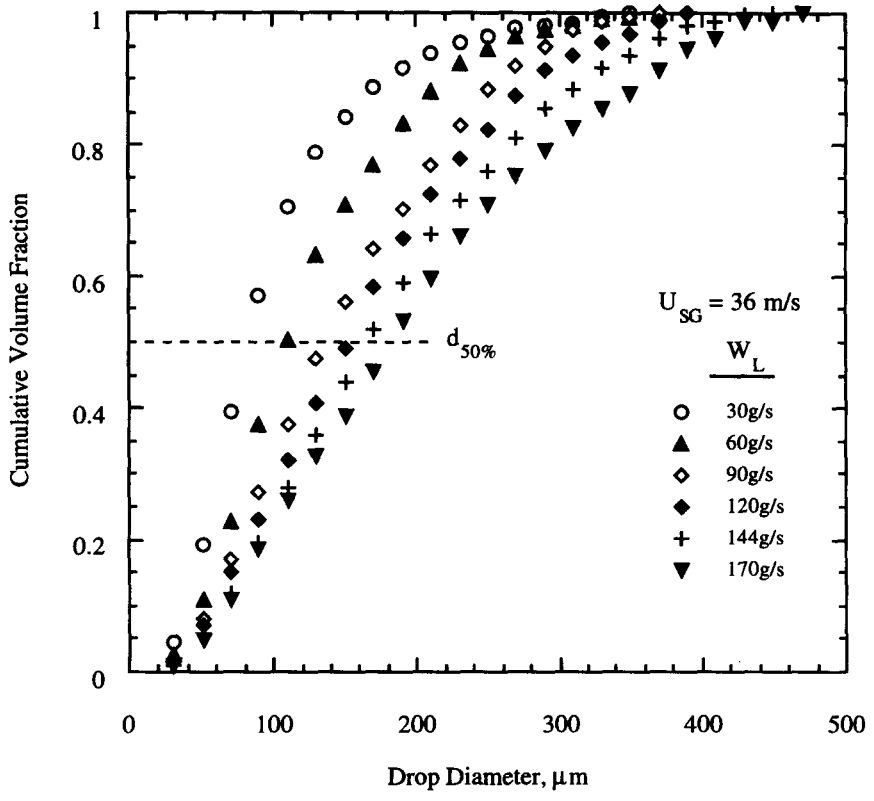

Figure 8. Cumulative volume fraction distributions.

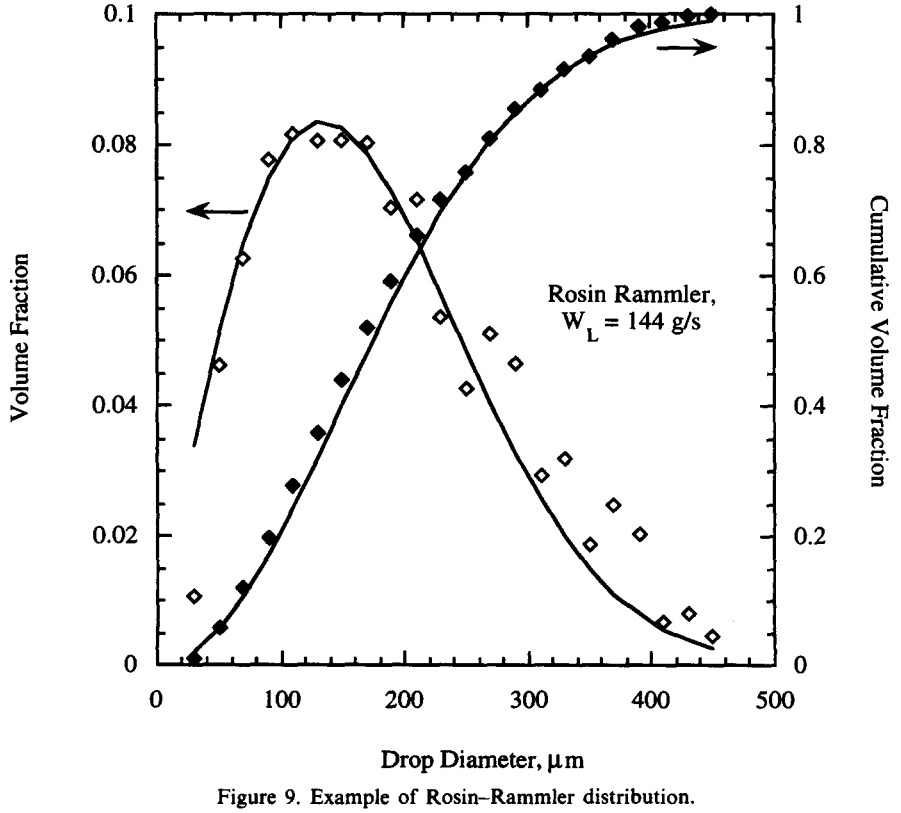

Figure 9. Example of Rosin–Rammler distribution.

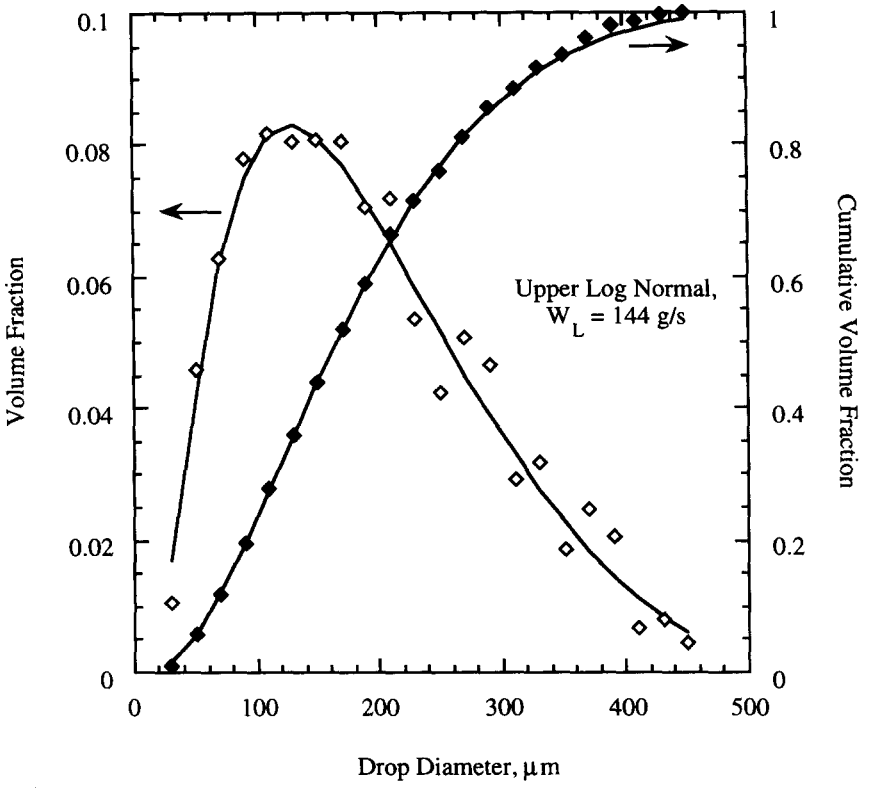

Figure 10. Example of upper limit log normal distribution.

presented in figure 11. Agreement is noted at low liquid flows. However, the measurements presented in this paper show a stronger effect of liquid flow. Somewhat better agreement is noted with the recent correlation suggested by Ambrosini *et al.* (1991). It is to be noted that most of the measurements considered by Azzopardi and by Ambrosini *et al.* depended on the use of a Rosin–Rammler distribution. If the measurements presented in this paper were fitted with a Rosin–Rammler distribution, the calculated Sauter mean diameters would lie between the correlations of Ambrosini *et al.* (1991) and Azzopardi (1985), except for the two lowest liquid flow rates where the Rosin–Rammler distribution describes the actual distribution poorly. Fore & Dukler (1995) also observed a larger effect of liquid flow than reported by Azzopardi. They reported a 70% increase with a four-fold increase in liquid flow for air superficial velocities in the range of 23–30 m/s. However, they obtained much larger Sauter mean diameters (400–750 μm) and observed almost no effect of gas velocity, in contrast to what has been observed by others. If one considers all of their data (18–33 m/s), a decrease of drop size with increasing gas velocity is noted.

One cause of the increase in drop size with increasing flow rate is coalescence. However, increasing liquid flows are also associated with thicker liquid films. This could lead to the formation of larger drops during atomization. The theory of Taylor (1940) suggests that drop size varies

Table 3. Upper limit and log normal distribution parameters

W_L (g/s)	δ	d_{rr} (μm)	d_m/d_{rr}	Equation
30	1.41	91.2	—	LN
60	1.26	121	—	LN
90	0.876	146	3.67	UL
120	0.833	161	3.31	UL
144	0.847	175	3.59	UL
170	0.810	192	3.85	UL
Average (UL)	0.84		3.6	

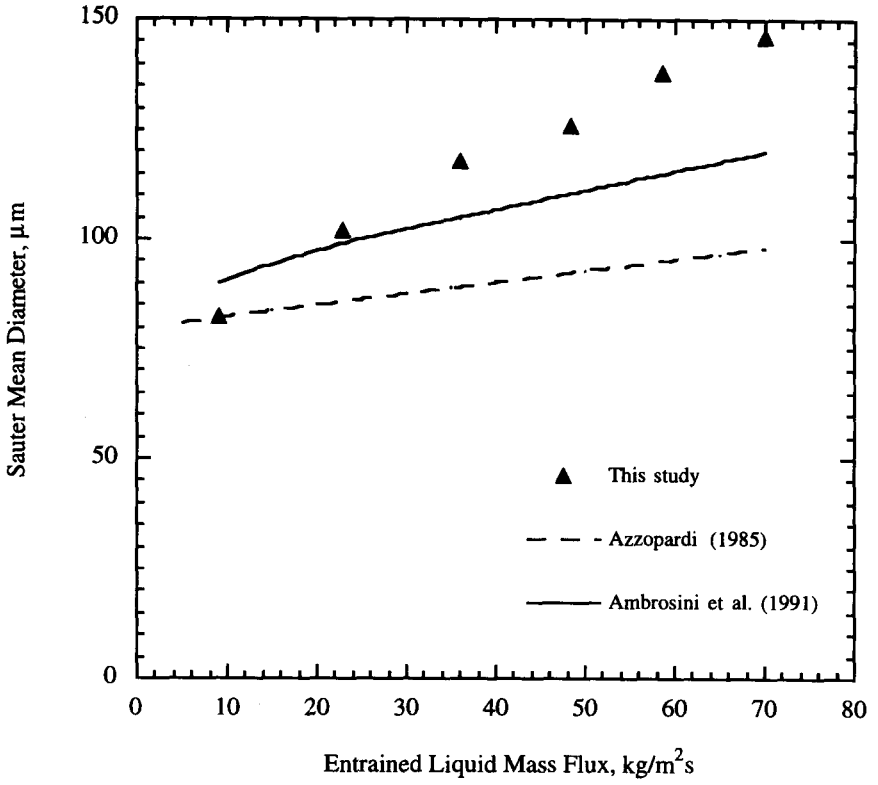

Figure 11. Sauter mean comparison to literature correlations.

directly with the wavelength of waves which are being removed from the liquid layer. If the wavelength scales with the thickness of the liquid film then one obtains

$$\frac{d_P}{m} = \text{constant.} \qquad [11]$$

Equation [11] is tested in figure 12 for d_{32}, d_{30} and for the median drop size. The correlation of Asali *et al.* (1985b) was used to calculate m for the different experimental conditions. The good agreement with [11] would suggest that an increase in the size of the film thickness during formation needs to be considered, along with coalescence, in explaining the increase in drop size with liquid flow.

4.3. Evolution of size distribution

One experiment was carried out, for a liquid flow of 144 g/s, at approximately half the axial distance ($z = 62$ pipe diameters) at which all of the other experiments were performed. A comparison of the two measured drop size distributions for $W_L = 144$ g/s is given in figure 13. The mass of entrained liquid at the two axial stations was approximately equal. Comparisons of the mean drop diameters are given in table 4. The increase in drop size with distance downstream suggests that coalescence could be occurring. However, it is also possible that some of the increase can be attributed to deposition. Larger drops will take longer times to deposit, so their numbers increase with increasing distance downstream.

5. COMPARISON WITH DILUTE SUSPENSION THEORY

The measurements of R_D in figure 3 and [3], developed for $C_B \approx C_W$, were used to calculate the change in particle turbulence. Figure 14 shows that values of $(\overline{v_p^2})^{1/2}$ obtained in this way approach a constant value, equal to about $0.18(\overline{v_f^2})^{1/2}$, at small concentrations and decrease as C^{-1} at large concentrations.

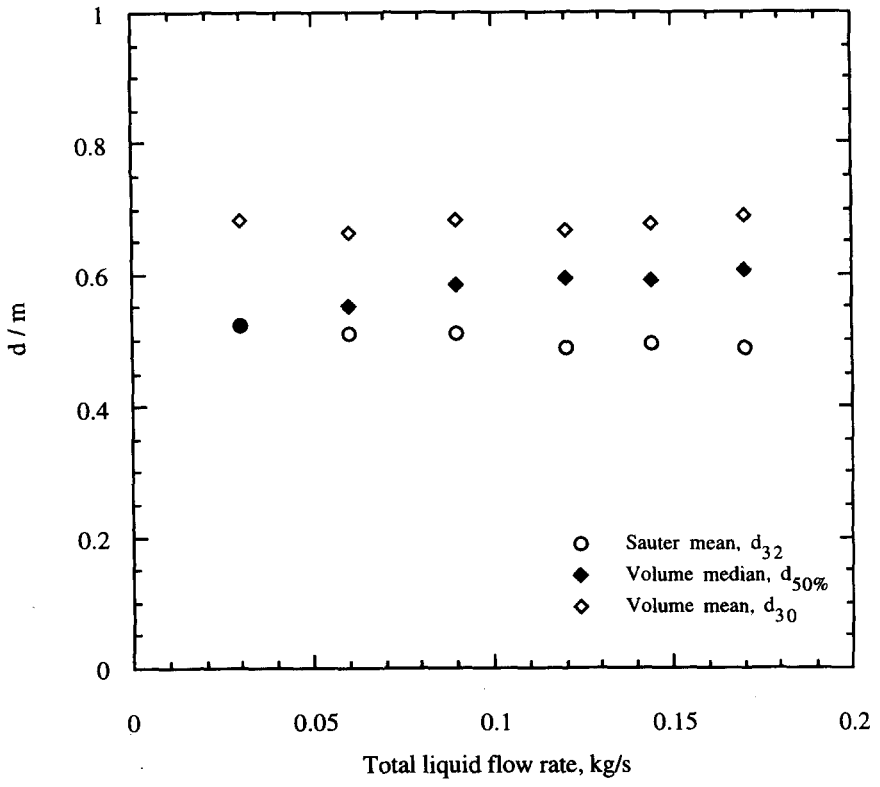

Figure 12. Scaling of drop size with average film thickness.

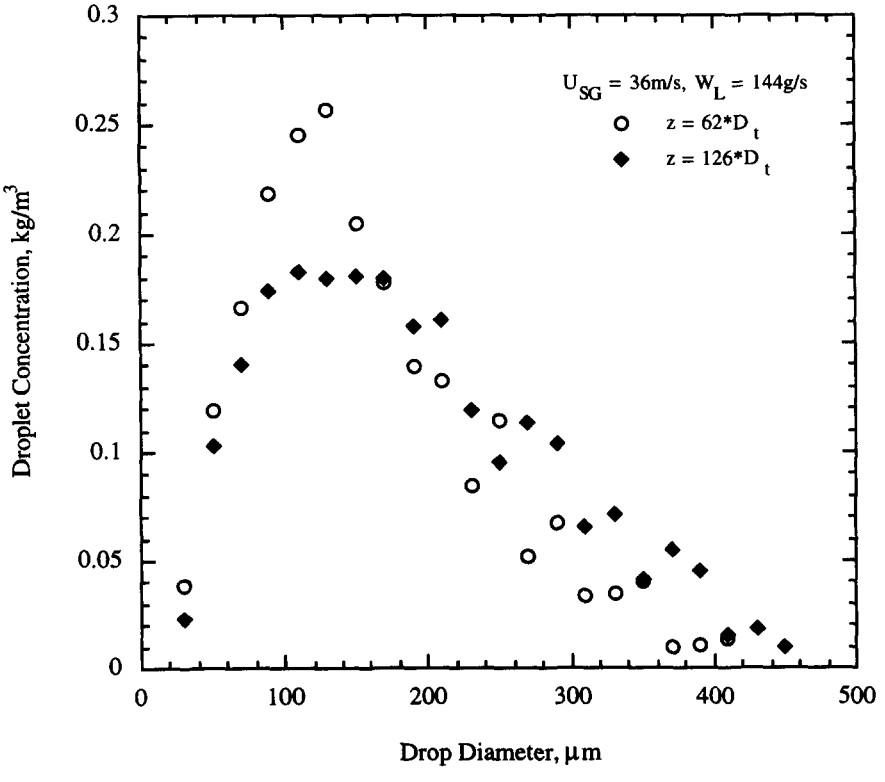

Figure 13. Development of drop distribution.

Table 4. Change in drop size between stations for $W_L = 144$ g/s

Mean diameter	$z = 62 \cdot D_t$ Size (μm)	$z = 126 \cdot D_t$ Size (μm)	% Increase between stations
d_{32}	120	138	15
d_{30}	160	189	18
$d_{50\%}$	133	165	24

Values of $(\overline{v_p^2})^{1/2}/(\overline{v_f^2})^{1/2}$, calculated with Reek's theory, are shown in figure 15. The solid curve shows the theoretical prediction for $V_S = 0$. The crosses represent measurements made by Lee *et al.* (1989b) for negligibly small V_S. Both the theory and experiments show a decrease in $(\overline{v_p^2})^{1/2}/(\overline{v_f^2})^{1/2}$ with decreasing $\beta\tau_{LF}$, because of increasing particle inertia. The dashed curve gives $\overline{v_p^2}/\overline{v_f^2}$ calculated with Reek's theory for $V_S/(\overline{v_f^2})^{1/2} = 3$. A decrease in $\overline{v_p^2}$ is indicated, because of the crossing-of-trajectories effect, first cited by Yudine (1959).

Values of $(\overline{v_p^2})^{1/2}/(\overline{v_f^2})^{1/2}$ have been calculated from the measured values of the Sauter mean diameters for $V_S = 0$, for V_S given by the free-fall velocity and for $V_S = (1 - S)U_{SG}$. Figure 14 shows that the calculated $\overline{v_p^2}$ are relatively insensitive to the model used for V_S (see Hay 1994 for detail). This is because increases in $\beta\tau_{LF}$ associated with increased drag tend to counterbalance the effect of an increase in $V_S/(\overline{v_f^2})^{1/2}$.

Rates of deposition calculated by using the drop size measurements, [2] and [3], and Reek's theory are shown in figure 16. In this calculation the relative contributions of the different sizes of drops were taken into account. The fluid turbulence was estimated as

$$(\overline{v_f^2})^{1/2} = 0.9u^*. \qquad [12]$$

Values of u^* measured by Asali *et al.* (1985b) and values of $\overline{v_f^2}$ calculated from [12] are presented in table 5 for each of the liquid flow rates that were studied. It is noted from figure 16 that good agreement is obtained with dilute suspension theory at the lowest liquid flow rate. However, dilute theory overpredicts the rate of deposition at large concentrations and the error becomes greater

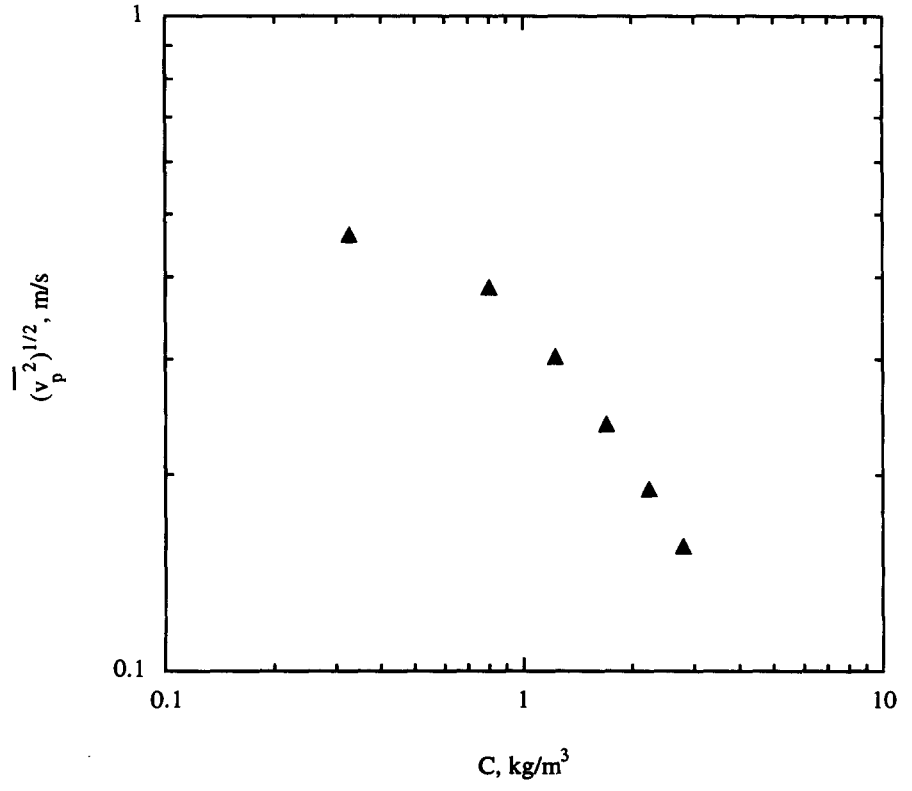

Figure 14. Root mean square particle velocity needed to explain deposition data.

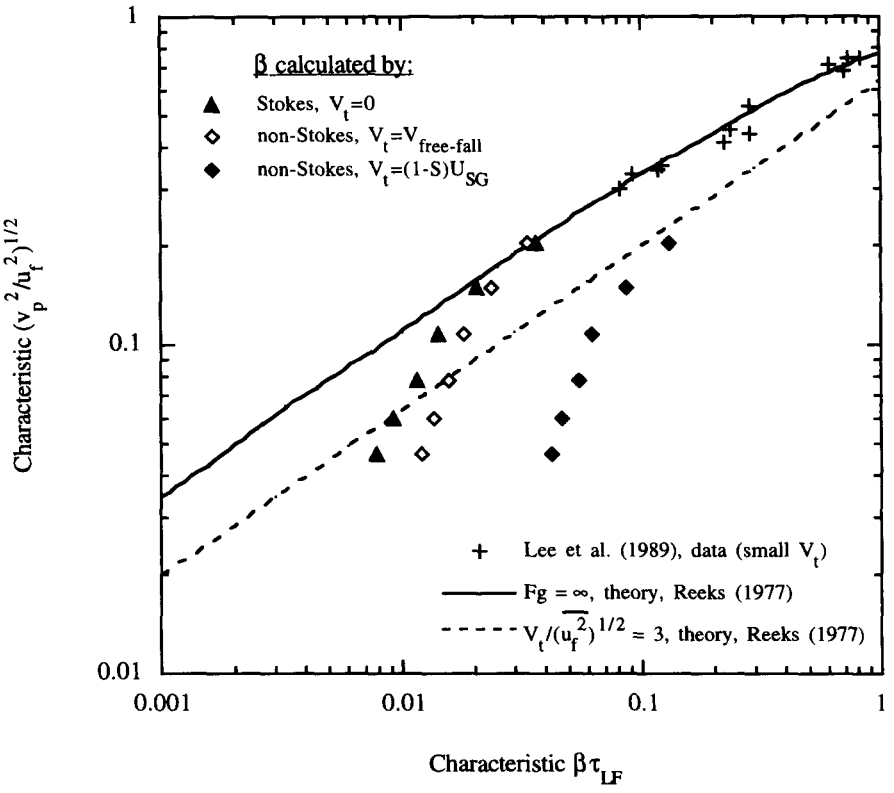

Figure 15. Predicted drop turbulence compared to literature.

with increasing concentration. These calculations show that the decreases of R_D with increasing liquid flow rate cannot be explained as resulting from increases in drop size.

6. INTERPRETATION

The above calculations show that deposition rates can be correctly calculated with [3] at low liquid flows by using theoretical estimates of $\overline{v_p^2}$ based on the behavior of a single particle in a turbulent fluid. The decrease in the deposition constant at large liquid flows, however, cannot be explained solely by an increase in drop size. Furthermore, measurements of gas phase velocity profiles shown in figure 6 do not support the notion that the decrease is associated with a decrease in the gas phase turbulence.

An important feature of the system studied is that the droplets are quite sluggish. The mean square of their velocity fluctuations, $\overline{v_p^2}$, is of the order of one per cent of the mean square of the fluid velocity fluctuations, $\overline{v_f^2}$. This would indicate that extraneous effects, other than fluid turbulence, could be important. Another feature is that, at large concentrations $(\overline{v_p^2})^{1/2}$ is varying as C^{-1}.

Since the number of encounters per unit time that a droplet experiences, n, increases linearly with the number of drops per unit volume, N, it is plausible to explore the notion that particle–particle encounters result in a decrease in particle turbulence through inelastic interactions.

Particle time scales are large compared to the turbulent time scales of the fluid. Therefore, a long time is needed for the particles to become fully entrained in the fluid turbulence. The small measured change in drop size along the pipe suggests that a surprisingly small fraction of the drop interactions results in coalescence (see Brown 1985). Suppose that the encounter of another drop most often results in an interruption of the radial motion of the drop. This temporarily decouples the particle from the fluid velocity field. Fluid turbulence again interacts with the particle and starts

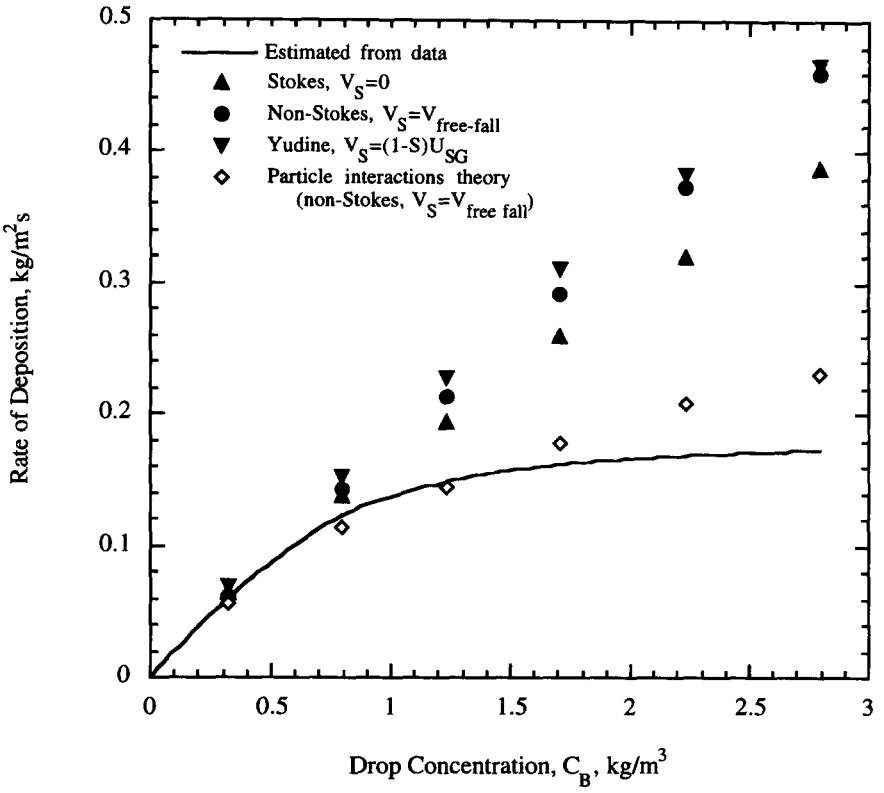

Figure 16. Theoretical predictions of the rate of deposition.

it on a new trajectory. The change of the particle velocity during this new trajectory is described by the equation.

$$\frac{dv_p}{dt} = \beta(v_f - v_p), \qquad [13]$$

where v_f and v_p are the radial velocity components of the fluid and the particle. Vames (1985) gives the following solution of [13]:

$$\overline{v_p^2} = \overline{v_{po}^2}\, e^{-2\beta t} + \frac{\overline{v_f^2}}{(\alpha+\beta)}[1 - e^{-2\beta t} - e^{-(\alpha+\beta)t} + e^{-(\alpha+3\beta)t}], \qquad [14]$$

where v_{p0} is the initial velocity of the drop. This result required the definition of a function, $R(t, \theta)$, which correlates the fluid velocity fluctuations seen by the particle at time t with the fluid velocity fluctuations seen at $(t + \theta)$. Equation [14] was derived by assuming

$$R(\theta) = \exp(-\alpha\theta), \qquad [15]$$

where α is a reciprocal time scale of the order of the reciprocal Lagrangian time scale of the fluid, that is determined empirically (see Vames & Hanratty 1988).

The average time interval between interactions, τ_i, is given as

$$\tau_i = n^{-1}. \qquad [16]$$

Table 5. Calculated gas phase velocities

W_L (g/s)	u^* (m/s)	$\overline{v_f^2}$ (m/s)^2
0	1.68	2.29
30	2.55	5.27
60	2.87	6.67
90	3.14	7.99
120	3.38	9.25
144	3.55	10.2
170	3.71	11.1

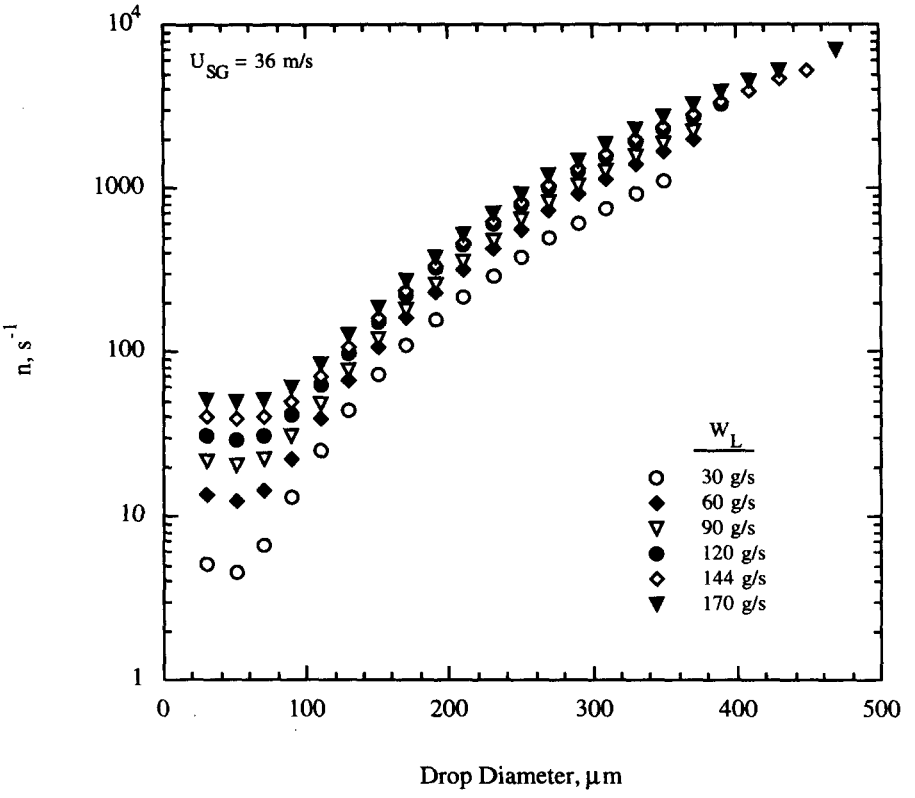

Figure 17. The number of encounters a drop of a given size will experience per unit time.

For large concentrations, $\beta\tau_i$ would be small. If $\overline{v_{p0}^2} \ll \overline{v_f^2}$ and $\beta \ll \alpha$, eqn [14] simplifies to

$$\overline{v_p^2} = 2t^2\beta^2\overline{v_f^2}. \quad [17]$$

This can be averaged over the time interval $t = 0$ to $t = \tau_i$ to obtain

$$\langle\overline{v_p^2}\rangle = \tfrac{2}{3}\tau_i^2\beta^2\overline{v_f^2} \quad [18]$$

or

$$\langle\overline{v_p^2}\rangle^{1/2} = \sqrt{\tfrac{2}{3}}n^{-1}\beta(\overline{v_f^2})^{1/2}. \quad [19]$$

Since $k_D \sim (\overline{v_p^2})^{1/2}$ and $n \sim C$, [19] gives $k_D \sim C^{-1}$ at large C.

In an attempt to quantify the impact of particle interactions on deposition an estimation of droplet encounter frequencies was made by Hay (1994). A brief outline of the computations is contained in appendix A. Particle encounters are assumed to occur due to the relative velocities between drops of different sizes caused by gravity. This could be a conservative estimate since effects to turbulence are neglected. The average velocity differences between drops of different sizes were approximated as equal to the differences in free-fall (terminal) velocities. The measurements of Teixeira (1988) indicate that the axial velocities of drops in an annular flow decrease with increasing drop size, at least in the order of the terminal velocity differences.

Results of the calculation performed by Hay are shown in figure 17. A larger drop sweeps through a continuous medium of smaller drops. Contributions from the interactions between all smaller and larger drops are summed to obtain the distribution of encounter frequencies, n, experienced by drops of different sizes. It is noted that n increases with increasing drop diameter and with increasing liquid flow.

Figure 17 and [14], with $v_{p0} = 0$ and $t = n^{-1}$, have been used to estimate deposition rates. The calculation is thus simplified by assuming that interacting drops reset to zero radial velocity regardless of drop size or velocity. The results are shown in figure 16 as open diamonds. It can be seen that calculated deposition rates are much closer to measurements than what is predicted by ignoring particle–particle interactions.

Acknowledgements—This work has been supported by the Department of Energy (Grant DEF G02-86ER 13556) and by the National Science Foundation (Grant NSF CTS 92-09877).

REFERENCES

Ambrosini, W., Andreussi, P. & Azzopardi, B. J. 1991 A physically based correlation for drop size in annular flow. *Int. J. Multiphase Flow* **17,** 497–507.

Anderson, G. H. & Mantzouranis, G. B. 1960 Two-phase flow phenomenon—I. *Chem. Eng. Science* **12,** 109–126.

Andreussi, P., Romano, G. & Zanelli, S. 1978 Drop size distribution in annular-mist flows. Presented at the *1st. Int. Conf. on Liquid Atomization and Spray Systems*, Tokyo.

Andreussi, P. & Zanelli, S. 1976 Liquid phase mass transfer in annular two-phase flow. *Ingegn. Chim.* **12,** 132–136.

Asali, J. C. 1984 Entrainment in vertical gas–liquid annular flows. Ph.D. thesis, University of Illinois, Urbana.

Asali, J. C., Leman, G. W. & Hanratty, T. J. 1985a Entrainment measurements and their use in design equations. *Physicochem. Hydrodynam.* **6,** 207–221.

Asali, J. C., Hanratty, T. J. & Andreussi P. 1985b Interfacial drag and film height for vertical annular flow. *AIChE J.* **31,** 895–902.

Azzopardi, B. J. 1985 Drop sizes in annular two-phase flow. *Expts Fluids* **3,** 53–59.

Azzopardi, B. J., Freeman, G. & Whalley, P. B. 1978 Drop sizes in annular two phase flow. UKAEA Report AERE-R9074.

Azzopardi, B. J., Freeman, G. & King, D. J. 1980 Drop sizes and deposition in annular two-phase flow. UKAEA Report AERE-R9634.

Azzopardi, B. J., Piearcey, A. & Jepson, D. M. 1991 Drop size measurements for annular two-phase flow in a 20 mm diameter vertical tube. *Expts Fluids* **11,** 191–197.

Azzopardi, B. J. & Teixeira, J. C. F. 1992 Gas core turbulence and drop velocities in vertical annular two phase flow. *28th National Heat Transfer Conf. and Exhibition*, San Diego, ASMFE HTV **197,** pp. 37–46.

Binder, J. L. & Hanratty, T. J. 1991 A diffusion model for droplet deposition in gas/liquid annular flow. *Int. J. Multiphase Flow* **17,** 1–11.

Brown, P. S. 1985 An implicit scheme for efficient solution of the coalescence/collision, break-up equation. *J. Comp. Physics* **58,** 417–431.

Fore, L. B. & Dukler, A. E. 1995 The distribution of drop size and velocity in gas–liquid annular flow. *Int. J. Multiphase Flow* **21,** 137–149.

Gill, L. E., Hewitt, G. F. & Lacey, P. M. C. 1964 Sampling probe studies of the gas core in annular two-phase flow. Part 2—studies of the effect of phase flow rates on phase and velocity distribution. *Chem. Eng. Sci.* **19,** 665–682.

Govan, A. H., Hewitt, G. F., Owen, D. G. & Bott, T. R. 1988 An improved CHF modelling code. Presented at the *2nd U.K. National Heat Transfer Conf.*, Strathclyde University, Glasgow.

Hay, K. J. 1994 The effect of drop concentration on deposition in vertical annular two-phase flow. Ph.D. thesis, University of Illinois, Urbana.

Jepson, D. M., Azzopardi, B. J. & Whalley, P. B. 1989 The effect of gas properties on drops in annular flow. *Int. J. Multiphase Flow* **15,** 327–339.

Lee, M. M., Hanratty, T. J. & Adrian, R. J. 1989a The interpretation of droplet deposition measurements with a diffusion model. *Int. J. Multiphase Flow* **15,** 459–469.

Lee, M. M., Hanratty, T. J. & Adrian, R. J. 1989b An axial viewing photographic technique to study turbulence characteristics of particles. *Int. J. Multiphase Flow* **15,** 787–802.

Lee, S. L. & Durst, F. 1982 On the motion of particles in turbulent duct flows. *Int. J. Multiphase Flow* **8,** 125.

Lopes, J. C. B. & Dukler, A. E. 1986 Droplet dynamics in vertical gas–liquid. *AIChE J.* **33,** 1013–1023.

Mei, R., Adrian, R. J. & Hanratty, T. J. 1993 Particle dispersion in isotropic turbulence under the influence of non-Stokesian drag and gravitational settling. Department of Theoretical and Applied Mechanics, University of Illinois, Urbana, TAM Report No. 735, UILU-ENG-93-6033.

Namie, S. & Ueda, T. 1972 Droplet transfer in two-phase annular mist flow. *Bull. J.S.M.E.* **15,** 1568.

Okada, O., Fujimatsu, T., Fujita, H. & Nakajima, Y. 1995 Measurement of droplet size distribution in an annular mist flow in a vertical pipe by immersion liquid method. *Proc. 2nd Int. Conf. Multiphase Flow*, Kyoto, 3–7 April 1995, pp. IP2–11.

Reeks, M. W. 1977 On the dispersion of small particles suspended in an isotropic turbulent fluid. *J. Fluid Mech.* **83,** 529–546.

Schadel, S. A., Leman, G. W., Binder, J. W. & Hanratty, T. J. 1990 Rates of atomization and deposition in vertical annular flow. *Int. J. Multiphase Flow* **16,** 363–374.

Schlichting, H. 1968 *Boundary-layer Theory*, 6th edn. MacGraw Hill, New York.

Semiat, R. & Duckler, A. E. 1981 Simultaneous measurement of size and velocity of bubbles or drops; a new optical technique. *AIChE J.* **27,** 148–159.

Tatterson, D. F., Dallman, J. C. & Hanratty, T. J. 1977 Drop size in annular gas liquid flows. *AIChE J.* **23,** 68–75.

Taylor, G. I. 1940 Generation of ripples by wind blowing over a viscous fluid. Reprinted in *The Scientific Papers of Sir Geoffrey Ingram Taylor*, Vol. 3. pp. 244–255. Cambridge University Press, London (1963).

Teixeira, J. C. F. 1988 Turbulence in annular two-phase flows. Ph.D. thesis, University of Birmingham, U.K.

Vames, J. C. 1985 Droplet dispersion in a turbulent pipe flow. Ph.D. thesis, University of Illinois, Urbana.

Vames, J. C. & Hanratty, T. J. 1988 Turbulent dispersion of droplets for air flow in a pipe. *Expts Fluids* **6,** 94–104.

Wicks, M. & Dukler, A. E. 1966 In situ measurements of drop size distributions in two phase flow: a new method for electrically conducting liquids. *Proc. 3rd Int. Heat Transfer Conf.* **5,** 39–48.

Williams, L. R. 1990 Effect of pipe diameter on horizontal annular flow. Ph.D. thesis, University of Illinois, Urbana.

Williams, L. R., Dykhno, L. A. & Hanratty, T. J. 1996 Droplet flux distributions and entrainment in horizontal gas–liquid flows. *Int. J. Multiphase Flow* **22,** 1–18.

Yudine, M. I. 1959 Physical consideration on heavy particle diffusion. *Adv. Geophys.* **6,** 185–191.

APPENDIX A

Particle encounter frequencies were determined by summing the number of interactions caused by differences in free-fall velocities. The radial velocities are assumed to equal zero. In the calculation, a uniform concentration of drops with a given size (designated as size distribution bin i) sweep out a volume containing a uniform concentration of smaller drops or are swept by a uniform concentration of large drops (j). The effective sweep volume rate of a drop is given by

$$Q_{ij} = \pi\left(\frac{d_i + d_j}{2}\right)^2 |v_i - v_j|, \qquad [A1]$$

where v is the free-fall velocity. The number concentration of drops can be expressed as $C/(\rho_L V_d)$, where C is the mass concentration and V_d is the spherical volume of a drop. The number of interactions per unit time experienced by an individual drop i with drops in bin j is given by

$$N_{ij} = Q_{ij}\frac{C_j}{\rho_L V_{dj}}. \qquad [A2]$$

The total number of interactions per unit time experienced by drop i is

$$n_i = \sum_{j=1}^{\#\text{ bins}} N_{ij}, \qquad [A3]$$

where it is noted that $N_{ii} = 0$.